Joint Denoising of Diffusion-Weighted Images via Structured Low-Rank Patch Matrix Approximation

Yujiao Zhao[1,2], Zheyuan Yi[1,2], Linfang Xiao[1,2], Vick Lau[1,2],

Yilong Liu[1,2], Zhe Zhang[3], Hua Guo[3], Alex T. Leong[1,2], and Ed X. Wu[1,2*]

[1]Laboratory of Biomedical Imaging and Signal Processing
The University of Hong Kong, Hong Kong SAR, People's Republic of China
[2]Department of Electrical and Electronic Engineering
The University of Hong Kong, Hong Kong SAR, People's Republic of China
[3]Center for Biomedical Imaging Research, Department of Biomedical Engineering
School of Medicine, Tsinghua University, Beijing, People's Republic of China

[*]Correspondence to:

Ed X. Wu, Ph.D.
Department of Electrical and Electronic Engineering
The University of Hong Kong, Hong Kong SAR, China
Tel: (852) 3917-7096
Fax: (852) 3917-8738
Email: ewu@eee.hku.hk

Short Running Title: Joint denoising DWIs via WNNM

Keywords: diffusion MRI, diffusion-weighted image, diffusion tensor imaging, patch matrix, low-rank approximation, weighted nuclear norm minimization

Zhao Y, Yi Z, Xiao L, Lau V, Liu Y, Zhang Z, Guo H, Leong AT, Wu EX. Joint denoising of diffusion-weighted images via structured low-rank patch matrix approximation. Magn Reson Med. 2022 Dec;88(6):2461-2474. doi: 10.1002/mrm.29407.

Abstract

Purpose: To develop a joint denoising method that effectively exploits natural information redundancy in MR diffusion-weighted images (DWIs) via low-rank patch matrix approximation.

Methods: A denoising method is introduced to jointly reduce noise in DWI dataset by exploiting non-local self-similarity as well as local anatomical/structural similarity within multiple 2D DWIs acquired with the same anatomical geometry but different diffusion directions. Specifically, for each small 3D reference patch sliding within 2D DWI, non-local but similar patches are searched by matching image contents within entire DWI dataset, and then structured into a patch matrix. The resulting patch matrices are denoised by enforcing low-rankness via weighted nuclear norm minimization, and finally back-distributed to DWI space. The proposed procedure was evaluated with simulated and in vivo brain diffusion tensor imaging (DTI) datasets, and compared to existing Marchenko-Pastur principal component analysis (MPPCA) denoising method.

Results: The proposed method achieved significant noise reduction while preserving structural details in all DWIs for both simulated and in vivo datasets. Quantitative evaluation of error maps demonstrated it consistently outperformed MPPCA method. Further, the denoised DWIs led to substantially improved DTI parametric maps, exhibiting significantly less noise and revealing more microstructural details.

Conclusion: The proposed method denoises DWI dataset by utilizing both non-local self-similarity and local structural similarity within DWI dataset. This WNNM based low-rank patch matrix denoising approach is effective and highly applicable to various diffusion MRI applications including DTI as a post-processing procedure.

Introduction

Diffusion MRI is a powerful imaging modality that provides non-invasive and quantitative characterization of tissue microstructures beyond image resolution[1]. However, diffusion-weighted images (DWIs) inherently suffer from low signal-to-noise ratio (SNR) due to signal attenuation by diffusion weighting and long echo time. This low SNR becomes more challenging when spatial resolution or/and diffusion weighting value (i.e., b-value) are high, which dramatically compromises DWI quality[2]. Moreover, such degradation can lead to inaccurate estimations in various types of diffusion parametric, tractography or connectivity analyses[2-4].

One approach to increase DWI SNR is through high-field or ultrahigh-field diffusion MRI[5-7], which in turn incurs trade-offs such as hardware costs and high-field related image artifacts[7]. Alternatively, the SNR can be enhanced by averaging but at the expenses of prolonged data acquisition time and vulnerability to subject motion[8]. Consequently, new diffusion MRI acquisition schemes such as simultaneous multi-slice protocols[9,10] have been developed to improve SNR without increasing data acquisition time.

On the other hand, denoising can be performed as a post-acquisition processing procedure to further boost DWI SNR[11-14]. For example, MR images including DWIs generally contain many repetitive or similar image content patterns (i.e., non-local self-similarity). Such information redundancy has been explored for anatomical image and DWI denoising in non-local means (NLM) based methods[13-15]. Specifically, sliding 2D patch is approximated by the simple weighted averaging of its non-local similar patches, through which the non-local self-similarity within a single DWI is partly utilized to reduce noise[14,15]. However, such NLM methods are often implemented to denoise individual DWIs[14,16]. Thus the extent of information redundancy utilization is limited. Further, the quality of searching for similar patches (i.e., patch matching) within individual 2D DWI can be compromised especially when SNR is low, likely hampering the denoising performance of NLM methods in terms of blurring or artifacts.

A typical diffusion MRI scan produces a multi-dimensional DWI dataset that consists of multiple DWIs acquired with the same anatomical geometry but different diffusion directions or/and diffusion weighting values. Despite the diffusion contrast differences,

the images within one DWI dataset often exhibit strong local image content similarity due to their shared anatomy and microstructures. From principal component analysis (PCA) point of view, such similarity allows local DWI contents to be decomposed into few signal-attributed principal components, whereas the noise is spread over all components due to its non-sparsity. PCA can therefore be adopted to denoise DWI dataset by nullifying the noise-only components[16-21]. Note that these PCA based diffusion MRI denoising methods are limited by the extent of local anatomical similarity, and their performance can be undermined if the DWI dataset does not provide sufficient redundancy (e.g., due to small number of diffusion directions)[21].

Specifically, the above PCA based diffusion MRI denoising methods leverage local anatomical similarity within an entire DWI dataset (i.e., DWIs with various diffusion directions or/and weightings) by low-rank approximation using rank truncation[16-21]. However, a target rank that distinguishes signal-attributed from noise-only components may not be easily obtained in practice when ground truth is not available. Early PCA based methods[18,19] empirically chose the rank truncation threshold with respect to image characteristics (e.g., spatial resolution and the number of diffusion directions or/and diffusion weighting values). Recently, Marchenko-Pastur PCA (MPPCA)[16,17] has been developed to estimate the rank truncation threshold by utilizing the fact that eigenvalues associated with noise-only components follow the universal Marchenko-Pastur distribution[22].

Intuitively, low-rank approximation approach can be formulated to denoise by exploiting *both* non-local *and* local similarities available in DWI dataset. Further, this approximation problem can be solved through nuclear norm minimization (NNM)[23]. NNM offers a convex relaxation to the low-rank approximation problem[24]. Compared to the aforementioned rank truncation based PCA denoising methods[16-19], low-rank approximation using NNM can lead to a globally optimal solution and meanwhile avoids the trial-and-error rank selection procedure[24].

In this study, we develop and demonstrate a new approach of jointly denoising DWI dataset acquired with different diffusion directions as in diffusion tensor imaging (DTI). The approach exploits both non-local self-similarity and local anatomical similarity within the entire DWI dataset through searching of non-local similar 3D patches, formation of patch matrices, and their low-rank approximations via a weighted NNM

(WNNM) procedure[25]. The proposed procedure effectively utilizes the information redundancy in DWI dataset. It produces significant noise reduction while preserving structural details for both simulated and in vivo brain DWI datasets. With such denoising, DWI datasets yield more accurate DTI parametric maps that exhibit less noise and reveal more microstructural details.

Methods

Joint DWI Denoising via Structured Low-Rank Patch Matrix Approximation

The proposed approach takes advantage of non-local self-similarity as well as local anatomical similarity within DWI dataset that consists of 2D DWIs acquired with the same slice geometry but different diffusion directions (including b-value = 0 image) by constructing low-rank patch matrices from the noisy DWIs, as shown in **Figure 1**. Joint denoising of DWIs is formulated as structured low-rank patch matrix denoising problem that is resolved by a WNNM[25] based procedure.

Formation of low-rank patch matrices: The proposed method exploits the information redundancy within DWI dataset by structuring patch matrices as follows. First, from $N_x \times N_y$ sized DWI dataset with N_d number of 2D DWIs (including image with b-value = 0), small 3D reference patches are formed by sliding the $n \times n \times N_d$ window across the entire 2D image region. For each reference patch P_0, as illustrated in **Figure 1**, non-local patches P_m (m = 1, 2, 3, …, M-1) containing similar image contents are searched by measuring the pixel-wise difference from the reference patch using Frobenius norm (i.e., patch matching)[13,26]. Here M represents the total number of non-local patches including the reference patch. Note that the similar patches are searched in the entire 2D image region instead of the local neighborhood around the reference patch. Then each reference patch P_0, together with its similar patches P_m, are stretched to vectors (y_0, y_1, y_2, …) in one dimension and then concatenated along the second dimension, forming a patch matrix Y with a size of $n^2 N_d \times M$.

As demonstrated in NLM based image denoising methods[13,14], individual MR image usually exhibits non-local self-similarity, which refers to the fact that, for a given reference patch, one can find many similar patches across the entire 2D image region.

This implies that, by stacking non-local similar patches from a single 2D DW image into a patch matrix, such patch matrix should be inherently low-rank[13,27]. Furthermore, given the local anatomical/structural similarity among DWIs, PCA based denoising methods have demonstrated that an individual local $n \times n \times N_d$ patch extracted from DWI dataset can be linearly represented with a small number of signal-attributed principal components[16,18,21]. From this perspective, the specific patch matrix Y constructed from multiple 2D DWIs in one DWI dataset (as shown in **Figure 1**) is expected to be more rank-deficient when compared to the patch matrix constructed from an individual DWI. The proposed patch matrix formation effectively promotes low-rankness of the patch matrices by explicitly exploiting all information redundancy in DWI dataset, including not only the non-local self-similarity in individual DWI but also the local structural similarity among all DWIs that correspond to different diffusion directions.

Denoising low-rank patch matrices via weighted nuclear norm minimization (WNNM): Given the low-rankness of patch matrices, joint denoising of DWIs can be formulated as a low-rank patch matrix approximation problem

$$\begin{aligned} &minimize\ rank(X) \\ &subject\ to\ \|Y - X\|_F^2 < \boldsymbol{\varepsilon} \end{aligned} \tag{1}$$

Here, Y is the original noisy patch matrix. X is the approximated noise-free patch matrix. $\|\cdot\|_F^2$ denotes the Frobenius norm, and ε determines the fidelity of the approximated patch matrix to the original patch matrix. Several early studies[23,24] have demonstrated that NNM can provide a convex relaxation to the low-rank approximation problem in Equation (1) and lead to a globally optimal solution via soft-thresholding the singular values of Y. However, in NNM, the soft-thresholding treats or shrinks all singular values equally, neglecting the prior knowledge that larger singular values usually represents more important signal-attributed components[28]. In this study, Equation (1) is reformulated using a weighted NNM (WNNM) model[25] as

$$\underset{X}{argmin}\ \|Y - X\|_F^2 + \|X\|_{\omega,*} \tag{2}$$

where $\|\cdot\|_{\omega,*}$ denotes weighted nuclear norm and is defined as weighted sum of singular values with non-negative weight vector ω.

Singular value decomposition (SVD) is employed to decompose patch matrix Y by deriving unitary matrices U and V, and diagonal matrix Σ with diagonal elements representing the singular values of Y as follows

$$Y = U\Sigma V^T \ . \tag{3}$$

After shrinking the singular values of patch matrix Y, a low-rank approximated patch matrix X is then obtained by

$$X \approx US_\omega(\Sigma)V^T \tag{4}$$

where $S_\omega(\cdot)$ is the singular value shrinkage operator with the weight vector ω

$$S_\omega(\Sigma_{ii}) = \max(\sigma_i - \omega_i, 0) \ . \tag{5}$$

Here, σ_i denotes the i-th diagonal element in Σ. ω_i denotes the i-th weight in ω[25], and is determined by

$$\omega_i = \frac{C}{\sqrt{\max\left(\sigma_i^2 - n^2 N_d M \delta^2, 0\right)} + \epsilon} \tag{6}$$

where δ is the noise level as determined by the standard deviation in individual DWIs. C is a positive constant and ϵ is a very small constant to avoid dividing by zero. Note that, since singular values are always sorted in a descending order, Equation (6) ensures that the weights assigned to singular values are ascending. On one hand, when the weights are non-descending, the solution in Equation (4) is a global optimum to the low-rank patch matrix approximation problem in Equation (2), as shown in previous WNNM study[25]. On the other hand, with the ascending weights, the singular value shrinkage procedure above leads to relatively less shrinkage of large singular values that represent major signal-attributed components, and causes more shrinkage of small singular values that correspond to noise-dominated components.

Back-distribution of patch matrices to image space: The above process of patch matrix formation and low-rank approximation is repeated for all 3D reference patches that slide across the entire 2D image region. As shown in **Figure 1**, denoised vectors (x_0, x_1,

x_2, …) in each denoised patch matrix X are back-distributed into the 3D reference and similar patches ($P_0', P_1', P_2', ...$) in DWI space. Note that final intensity of each DWI pixel is normalized by number of back-distributions to that specific pixel throughout the entire procedure.

Experiments

The proposed denoising method was first evaluated using simulated human brain datasets. Brain-like phantom created for ISMRM 2015 Tractography challenge[29] was used to generate brain DWI dataset[30] with matrix size = 90×108×90, isotropic resolution = 2 mm, one b-value = 0 image and 30 diffusion directions with b-value = 1000 and 2000 s/mm^2. For evaluation, two datasets were synthesized by extracting 6 DWIs from the simulated dataset with b-value = 1000 and 2000 s/mm^2, respectively. The b-value = 0 image was also included in each dataset to form two ground truth DWI datasets. Each dataset contained a total of 7 images. Noisy DWI datasets were obtained by adding Rician noise to the ground truth magnitude DWIs. The noise level was quantified using the percentage ratio of standard deviation of the underlying Gaussian noise in complex domain to the maximum image intensity in ground truth DWI dataset (i.e., CSF intensity in b-value = 0 image).

The proposed method was also evaluated with in vivo human brain DWI datasets acquired on a 3T Philips scanner (Achieva, Philips Medical Systems, Best, The Netherlands). All experiments involving human subjects were approved by the local institutional board and written information consents were obtained. Specifically, two brain DWI/DTI datasets were acquired using an 8-channel head coil and 4-shot interleaved 2D EPI DWI protocol with matrix size = 220×220, in-plane resolution = 1×1 mm^2, slice number = 10 and slice thickness = 4 mm. The scan parameters for the first dataset were TR/TE = 2500/123 ms, one b-value = 0 image with NEX = 1, and 6 diffusion directions with b-value = 1000/2000/3000 s/mm^2 and each with NEX = 4. The scan parameters for the second dataset were TR/TE = 2400/118 ms, one b-value = 0 image with NEX = 1, and 6 diffusion directions with b-value = 2000 s/mm^2 and each with NEX = 10. POCSMUSE[31] reconstruction method was applied for both datasets. The reconstructed single-average datasets were used as noisy datasets for evaluating the denoising method. Meanwhile, in vivo datasets with NEX of 10 or 4 were employed

as references for comparison.

The proposed denoising method was applied to the multi-slice 2D DWI datasets in a slice-by-slice manner. Several denoising parameters were adjusted for simulated and in vivo datasets. Specifically, the patch window size of the reference patches was chosen to be $n \times n = 3 \times 3$ and 6×6 for simulated and in vivo brain datasets, respectively, with $N_d = 7$ unless specified otherwise. This difference was due to their different image resolutions. The reference patch sliding step and patching search step were set to 2 and 3 in both directions for simulated and in vivo datasets, respectively, for simplicity as well as for lessening the computational burden. The number of similar patches (including the reference patch itself) was set to $M = 60$ and 140 for simulated and in vivo brain datasets, respectively. Constants C and ϵ in Equation (6) were fixed to 2.8 and 10^{-16}, respectively.

For comparison, the denoising was also performed using the widely adopted MPPCA[16,17] (https://github.com/NYU-DiffusionMRI/mppca_denoise), which has been shown to be highly effective in denoising DWI dataset. MPPCA was implemented using a sliding window of $n \times n \times n \times N_d$ voxels, with the 3rd dimension corresponding to samples from all neighboring slices (since MPPCA is a 3D denoising method). Here $n \times n \times n$ was set to $3 \times 3 \times 3$ and $6 \times 6 \times 6$ for simulated and in vivo datasets, respectively. Given that MPPCA denoising requires sufficient local anatomical redundancy (e.g., from a large number of diffusion directions), adaptive NLM (ANLM)[15] was also implemented for comparison when denoising DWI datasets with relatively few diffusion directions. Unlike MPPCA and the proposed method, ANLM was applied on individual DWIs with default $3 \times 3 \times 3$ sliding window and $7 \times 7 \times 7$ searching volume.

FSL DTIFit Toolbox[32] was employed to derive DTI parametric maps, i.e., mean diffusivity (MD), fractional anisotropy (FA) and mean kurtosis (MK). The color-encoded FA maps were also computed to indicate the orientation of the principal eigenvector, with red corresponding to right-left, green corresponding to anterior-posterior and blue corresponding to superior-inferior. The error or difference maps were calculated by subtracting denoised images from ground truth images or reference images (with NEX = 4 or 10) for simulated or in vivo results, respectively. Relative bias and normalized root-mean-square errors (NRMSEs) within brain region were measured to assess the denoising performance. For color-encoded FA maps, the bias

and NRMSEs were calculated from error or difference vectors.

Our proposed denoising algorithm and evaluation above were implemented using MatLab (MathWorks, Natick, MA). All source code can be obtained online (https://github.com/joey024/DWIdenoising) or from the authors upon request.

Results

The typical denoising results of simulated brain DWI/DTI dataset with 2% noise level are shown in **Figure 2**. One b-value = 0 and 6 b-value = 1000 s/mm^2 images were jointly denoised. The proposed method achieved effective noise reduction. Compared to MPPCA results, about 30% more NRMSE reduction was obtained. **Supporting Information Figure S1** presents the influence of patch window size *n* on the proposed method and MPPCA when denoising the results in **Figure 2**. Although the performance of both methods could be degraded with increasing window sizes, the proposed method yielded smaller NRMSEs than MPPCA. The improved denoising results using the proposed method led to more accurate diffusion parametric maps, exhibiting less noise and revealing more microstructural details in both FA intensity maps and color-encoded FA maps (**Figure 2**). Quantitative evaluation further demonstrated that the proposed denoising results achieved higher levels of agreement with ground truth for various parametric maps in terms of smaller bias and NRMSEs.

Figure 3 shows the denoising results of simulated brain DWI dataset that consisted of one b-value = 0 and 6 b-value = 2000 s/mm^2 images with 2% noise level. Note that, in presence of low SNR, FA estimation directly from noise-added DWIs completely failed. With MPPCA denoising, improved FA maps could be obtained. However, with the proposed method, the noise in DWIs was more effectively reduced, leading to significantly improved diffusion parametric maps with considerably smaller bias and NRMSEs.

As shown in **Supporting Information Figure S2**, for simulated brain DWI datasets with an increased number of diffusion directions, both MPPCA and the proposed denoising results were improved when compared to those with only 6 diffusion directions (**Figures 2** and **3**). Nevertheless, the proposed method could still achieve

higher noise reduction than MPPCA, even in presence of Gaussian distributed noise (i.e., when the noise assumption of MPPCA was satisfied; see **Supporting Information Figure S3**). These simulated results demonstrated that the proposed denoising method was highly effective and robust.

Figure 4 presents the typical denoising results of in vivo brain DWI dataset. One b-value = 0 and 6 b-value = 1000 s/mm^2 images (in 6 directions) were jointly denoised. The proposed method yielded an approximately 25% NRMSE reduction in denoised DWIs compared to MPPCA. No apparent anatomical structure was observed in the difference images, suggesting that the structural details were largely preserved in the proposed denoising. Consistent with the simulation experiments, the more effective DWI noise reduction using the proposed method yielded improved diffusion parametric maps. As shown in **Figure 5**, with MPPCA denoising, microstructural detail loss could be clearly observed in the FA and color-encoded FA maps as indicated by red and white arrows, respectively. In contrast, with the proposed denoising, more microstructural details were revealed.

Figure 6 compares the proposed and MPPCA denoising of in vivo brain DWI dataset that consisted of one b-value = 0 and 6 b-value = 2000 s/mm^2 images. Again, the proposed method outperformed MPPCA in terms of smaller NRMSEs for denoised DWIs and diffusion parametric maps. As shown in the zoomed view (**Figure 7**), distinct noise was still present in MPPCA denoised DWI, but largely absent in DWI denoised using our proposed method. With the proposed denoising, the FA and color-encoded FA maps revealed more microstructural details (indicated by arrows), and their quality was comparable to NEX = 4 reference results. Note that both MPPCA and the proposed method resulted in better preservation of structural details when compared to single-DWI denoising using ANLM (see **Supporting Information Figures S4 and S5**). **Supporting Information Figures S6 and S7** present denoising results of the same dataset at two other slice locations. These results demonstrated that, at low SNR, the proposed method was consistently more effective than MPPCA.

The denoising results of in vivo brain multi-shell DWI dataset are shown in **Figure 8**. The dataset consisted of one b-value = 0 image, and 6 diffusion directions with b-value = 1000/2000/3000 s/mm^2 (i.e., a total of 19 images). With MPPCA denoising, noise in the b-value = 1000 s/mm^2 images were significantly reduced, whereas distinct residual

noise were still present in the b-value = 2000/3000 s/mm^2 images (including the DWIs averaged from 6 diffusion directions per b-value). In contrast, the proposed method achieved more effective noise reduction in all DWIs, with approximately zero bias and 20% more NRMSE reduction when compared to MPPCA. The denoised DWIs using the proposed method led to more accurate diffusion parametric maps, exhibiting less noise and becoming more comparable to the NEX = 4 reference (**Supporting Information Figure S8**).

The influence of reducing diffusion direction number (i.e., reduced extent of local anatomical similarity) on joint DWI denoising is shown in **Figure 9**. One b-value = 0 and 3 b-value = 2000 s/mm^2 images (in 3 orthogonal directions) were extracted from the DWI dataset used for **Figure 6** and jointly denoised. This evaluation is relevant to some simple clinical DWI scenarios where, for example, single DWI with isotropic diffusion weighting is formed from three DWIs acquired in three orthogonal diffusion directions. Here the proposed method was compared with ANLM because MPPCA was expected to become less effective due to the relatively small diffusion direction number. For ANLM denoising, when SNR was low, the results would exhibit pronounced blurring. Such blurring caused structural detail loss, and presented as anatomical structure in difference maps, leading to a large bias in denoised DWIs and MD maps. However, with the proposed denoising, the noise was effectively reduced while the structural details were well preserved, yielding a substantial reduction in both bias and NRMSEs.

Supporting Information Figure S9 illustrates the tolerance of our proposed method to the minor spatial misalignments among DWIs. Simulated misalignments were introduced to the in vivo DWI dataset by manually shifting the b-value = 2000 s/mm^2 DWI shown in **Figure 6** by 1, 3 or 5 pixels (corresponding to 1 mm, 3 mm or 5 mm) in right-left direction. With 1-pixel displacement, MPPCA exhibited slightly degraded denoising performance compared to that without any displacement. For the proposed method, the degradation was negligible. With relatively larger displacement (3-pixel or 5-pixel), the degradation of MPPCA denoising became more pronounced and led to more residual noise with NRMSE increased by ~10% compared to that without any displacement. Such performance degradation was largely expected because MPPCA denoising solely relies on the local structural similarity among DWIs, which can

severely deteriorate in presence of large spatial misalignment. Meanwhile, the denoising using the proposed method exhibited relatively little changes as evident from both image details and NRMSEs, indicating that it was less sensitive to such spatial misalignments among DWIs.

Discussion

This study presents a new approach for jointly denoising DWI dataset acquired with different diffusion directions through a WNNM based low-rank patch matrix denoising procedure. We have demonstrated that the proposed method produces significant and robust noise reduction while preserving structural details. The proposed denoising also leads to more accurate DTI parametric maps that exhibit less noise and reveal more microstructural details.

Existing PCA based denoising methods such as MPPCA[16-18,21] usually utilize local anatomical similarity or redundancy within one DWI dataset only. Our proposed method exploits both local structural similarity and non-local self-similarity within the DWI dataset. In this regard, it enables more effective exploitation of the information redundancy. It outperforms existing MPPCA method as demonstrated in the present study (despite MPPCA exploits the local structural similarity directly in a 3D manner; see **Figure 8**, and **Supporting Information Figures S2 and S3**). More importantly, the proposed method works effectively and robustly for DWI datasets with a small number of diffusion directions, where many existing PCA based methods would exhibit degraded denoising performance due to the insufficient local anatomical redundancy (see Figures 2, 3, 4, and 6). Therefore, it is highly applicable to clinical diffusion MRI applications in which a large number of diffusion directions and/or b-values are often unavailable due to the acquisition time consideration.

The proposed approach jointly reduces noise in DWI dataset by low-rank patch matrix approximation via the WNNM procedure. Previous study has revealed that WNNM has a globally optimal solution to the low-rank matrix approximation problem if the weights assigned to singular values are in a non-descending order[25]. In this study, the weights were imposed to be inversely proportional to singular values by Equation (4), thus an optimal solution to the low-rank patch matrix approximation was guaranteed, in

contrast to the largely ad hoc approximations in previous methods where simple rank truncation is adopted[16-19]. Additionally, the non-descending weights allow larger singular values (i.e., represent major signal-attributed components) to be less shrunk during the matrix approximation[25], indicating that more reliable denoising can be achieved.

In practice, the performance of our proposed method can be influenced by the patch searching parameters (i.e., patch window size and patch sliding step). As shown in **Supporting Information Figure S1**, despite that the overall image quality of the proposed denoising results was better than that of MPPCA results, it could be degraded when a large patch window size was employed. This was because the patch with large window size may capture more specific structural details (i.e., increased complexity or diversity of image contents[33]) but less non-local self-similarity details, thus undermining the overall 3D patch matching quality. In addition, a larger patch sliding step could result in non-overlapping reference patches and cause residual noise around the patch boundaries[27]. Note that large patch window size or/and small patch sliding step will greatly increase computation load. In this study, these two parameters were empirically chosen based on the image resolutions.

Subject involuntary motion, as well as hardware imperfections (e.g., eddy current induced image distortions[34]), can often introduce small but non-negligible rigid and non-rigid spatial misalignments among DWIs. Such misalignments can complicate or degrade the performance of the joint denoising strategies such as MPPCA and our proposed method. Various approaches have been developed and adopted in practical diffusion MRI to mitigate this misalignment problem[34-36], and they can be performed before the joint DWI dataset denoising. Importantly, the present study has demonstrated that, without realignment, the proposed method could still achieve promising noise reduction and outperform MPPCA in presence of minor misalignments among DWIs (**Supporting Information Figure S9**). This observation indicates the lesser degree of vulnerability of the proposed method to spatial misalignments. This is expected because the method utilizes both non-local and local similarities while extent of non-local similarity within DWIs should preserve despite the misalignments. In advanced diffusion MRI applications beyond 6-direction DTI demonstrated in the present study, individual DWIs may have different overall noise levels (e.g., due to different averages).

In such scenarios, additional weighting matrix[37] determined by the noise levels can be assigned to the patch matrix. By this means, the noise level differences are balanced and DWIs with lower noise levels will make more contribution during the patch matrix approximation via WNNM[37].

In this study, multi-slice 2D DWIs were denoised jointly for different diffusion directions, but in a slice-by-slice manner. Intuitively, multi-slice DWI dataset can exhibit higher level of non-local 3D self-similarity especially when voxel resolution is isotropic. In this regard, the proposed method could be potentially extended to jointly denoising the entire 3D DWIs by adopting a strategy of 4D patch searching across 3D DWI space, appropriate low-rank patch matrix formation, and patch matrix denoising through low-rank approximation. This strategy would incur much higher computational cost, yet we would expect that it can exploit the non-local and local 3D information redundancy with the entire 3D DWI dataset, and lead to further improved denoising performance. This will be a direction to pursue in future studies.

It is noteworthy to mention the potentially broad applicability of the proposed denoising method. The present study demonstrated that the superior performance of our method does not heavily rely on large number of DWIs (**Figure 9**), or presence of any high SNR DWI (such as b-value = 0 image; see **Supporting Information Figure S10**). This suggests that the method can be applied to other clinical MRI protocols besides diffusion MRI. In our earlier preliminary study, we suggested that the proposed low-rank patch matrix approximation approach could jointly denoise multi-contrast MRI images while preserving structural details even in presence of brain pathology[38]. Future studies can further evaluate such framework for other MRI applications beyond DTI, such as multi-echo T2 or T2* mapping or dynamic imaging.

The proposed method was implemented on a personal desktop computer equipped with 4-core i5-6500 CPU and 16-GB RAM. For in vivo brain DWI dataset with matrix size = 220×220 and one b-value = 0 and 6 b-value = 2000 s/mm^2 images, the denoising with patch window size 6×6 took about 4 minutes per slice. To accelerate the computation, the denoising can be implemented with high-performance GPU-based computing[39].

Conclusion

This study presents a novel approach for jointly denoising DWI dataset acquired with different diffusion directions. It explicitly exploits both non-local self-similarity and local anatomical similarity within the DWI dataset, yielding significant noise reduction while preserving structural details. With the proposed denoising, DWI datasets also lead to more accurate DTI parametric maps, exhibiting significantly less noise and revealing more microstructural details. This WNNM based low-rank patch matrix denoising approach is effective and highly applicable to various diffusion MRI applications including DTI as a post-processing procedure.

Acknowledgments

This study is supported in part by Hong Kong Research Grant Council (R7003-19, HKU17112120 and HKU17127121 to E.X.W. and HKU17103819, HKU17104020 and HKU17127021 to A.T.L.), and Lam Woo Foundation. We thank Mr. Xinyu Ye for technical assistance.

Reference

[1] Jones DK. Diffusion MRI: Oxford University Press; 2010.

[2] Jones DK, Basser PJ. “Squashing peanuts and smashing pumpkins”: how noise distorts diffusion-weighted MR data. Magn Reson Med 2004;52(5):979-993.

[3] Huang H, Zhang J, Van Zijl PC, Mori S. Analysis of noise effects on DTI-based tractography using the brute-force and multi-ROI approach. Magn Reson Med 2004;52(3):559-565.

[4] Lori N, Akbudak E, Shimony J, Cull T, Snyder A, Guillory R, Conturo T. Diffusion tensor fiber tracking of human brain connectivity: aquisition methods, reliability analysis and biological results. NMR Biomed 2002;15(7-8):494-515.

[5] Strotmann B, Heidemann RM, Anwander A, Weiss M, Trampel R, Villringer A, Turner R. High-resolution MRI and diffusion-weighted imaging of the human habenula at 7 tesla. J Magn Reson Imaging 2014;39(4):1018-1026.

[6] Kleinnijenhuis M, van Mourik T, Norris DG, Ruiter DJ, van Walsum A-MvC, Barth M. Diffusion tensor characteristics of gyrencephaly using high resolution diffusion MRI in vivo at 7T. NeuroImage 2015;109:378-387.

[7] Gallichan D. Diffusion MRI of the human brain at ultra-high field (UHF): A review. NeuroImage 2018;168:172-180.

[8] Eichner C, Cauley SF, Cohen-Adad J, Möller HE, Turner R, Setsompop K, Wald LL. Real diffusion-weighted MRI enabling true signal averaging and increased diffusion contrast. NeuroImage 2015;122:373-384.

[9] Setsompop K, Cohen-Adad J, Gagoski BA, Raij T, Yendiki A, Keil B, Wedeen VJ, Wald LL. Improving diffusion MRI using simultaneous multi-slice echo planar imaging. NeuroImage 2012;63(1):569-580.

[10] Setsompop K, Fan Q, Stockmann J, Bilgic B, Huang S, Cauley SF, Nummenmaa A, Wang F, Rathi Y, Witzel T. High-resolution in vivo diffusion imaging of the human brain with generalized slice dithered enhanced resolution: Simultaneous multislice (gSlider-SMS). Magn Reson Med 2018;79(1):141-151.

[11] Wirestam R, Bibic A, Lätt J, Brockstedt S, Ståhlberg F. Denoising of complex MRI data by wavelet-domain filtering: Application to high-b-value diffusion-weighted imaging. Magn Reson Med 2006;56(5):1114-1120.

[12] Knoll F, Bredies K, Pock T, Stollberger R. Second order total generalized variation (TGV) for MRI. Magn Reson Med 2011;65(2):480-491.

[13] Coupé P, Yger P, Prima S, Hellier P, Kervrann C, Barillot C. An optimized blockwise nonlocal means denoising filter for 3-D magnetic resonance images.

IEEE Trans Med Imaging 2008;27(4):425-441.

[14] Wiest-Daesslé N, Prima S, Coupé P, Morrissey SP, Barillot C. Non-local means variants for denoising of diffusion-weighted and diffusion tensor MRI. In: Med Image Comput Comput Assist Interv, 2007, p 344-351.

[15] Manjon JV, Coupe P, Marti-Bonmati L, Collins DL, Robles M. Adaptive non-local means denoising of MR images with spatially varying noise levels. J Magn Reson Imaging 2010;31(1):192-203.

[16] Veraart J, Novikov DS, Christiaens D, Ades-Aron B, Sijbers J, Fieremans E. Denoising of diffusion MRI using random matrix theory. NeuroImage 2016;142:394-406.

[17] Veraart J, Fieremans E, Novikov DS. Diffusion MRI noise mapping using random matrix theory. Magn Reson Med 2016;76(5):1582-1593.

[18] Manjón JV, Coupé P, Concha L, Buades A, Collins DL, Robles M. Diffusion weighted image denoising using overcomplete local PCA. PloS one 2013;8(9):e73021.

[19] Manjón JV, Coupé P, Buades A. MRI noise estimation and denoising using non-local PCA. Med Image Anal 2015;22(1):35-47.

[20] Cordero-Grande L, Christiaens D, Hutter J, Price AN, Hajnal JV. Complex diffusion-weighted image estimation via matrix recovery under general noise models. NeuroImage 2019;200:391-404.

[21] Ramos-Llordén G, Vegas-Sánchez-Ferrero G, Liao C, Westin CF, Setsompop K, Rathi Y. SNR-enhanced diffusion MRI with structure-preserving low-rank denoising in reproducing kernel Hilbert spaces. Magn Reson Med 2021;86(3):1614-1632.

[22] Marchenko VA, Pastur LA. Distribution of eigenvalues for some sets of random matrices. Matematicheskii Sbornik 1967;114(4):507-536.

[23] Candès EJ, Recht B. Exact matrix completion via convex optimization. Foundations of Computational mathematics 2009;9(6):717-772.

[24] Cai J-F, Candès EJ, Shen Z. A singular value thresholding algorithm for matrix completion. SIAM Journal on optimization 2010;20(4):1956-1982.

[25] Gu S, Zhang L, Zuo W, Feng X. Weighted nuclear norm minimization with application to image denoising. In: Proc IEEE Comput Soc Conf Comput Vis Pattern Recognit, 2014, p 2862-2869.

[26] Dabov K, Foi A, Katkovnik V, Egiazarian K. Image denoising by sparse 3-D transform-domain collaborative filtering. IEEE Trans Image Process 2007;16(8):2080-2095.

[27] Guo S, Fessler JA, Noll DC. High-Resolution Oscillating Steady-State fMRI Using Patch-Tensor Low-Rank Reconstruction. IEEE Trans Med Imaging

2020;39(12):4357-4368.

[28] Gavish M, Donoho DL. Optimal shrinkage of singular values. IEEE Trans Inf Theory 2017;63(4):2137-2152.

[29] Neher PF, Laun FB, Stieltjes B, Maier-Hein KH. Fiberfox: facilitating the creation of realistic white matter software phantoms. Magn Reson Med 2014;72(5):1460-1470.

[30] Ma X, Uğurbil K, Wu X. Denoise magnitude diffusion magnetic resonance images via variance-stabilizing transformation and optimal singular-value manipulation. NeuroImage 2020;215:116852.

[31] Chu ML, Chang HC, Chung HW, Truong TK, Bashir MR, Chen Nk. POCS-based reconstruction of multiplexed sensitivity encoded MRI (POCSMUSE): a general algorithm for reducing motion-related artifacts. Magn Reson Med 2015;74(5):1336-1348.

[32] Jenkinson M, Beckmann CF, Behrens TE, Woolrich MW, Smith SM. FSL. NeuroImage 2012;62(2):782-790.

[33] Levin A, Nadler B, Durand F, Freeman WT. Patch complexity, finite pixel correlations and optimal denoising. In: Computer Vis ECCV, 2012, p 73-86.

[34] Irfanoglu MO, Sarlls J, Nayak A, Pierpaoli C. Evaluating corrections for Eddy-currents and other EPI distortions in diffusion MRI: methodology and a dataset for benchmarking. Magn Reson Med 2019;81(4):2774-2787.

[35] Rohde GK, Barnett A, Basser P, Marenco S, Pierpaoli C. Comprehensive approach for correction of motion and distortion in diffusion-weighted MRI. Magn Reson Med 2004;51(1):103-114.

[36] Jones DK, Cercignani M. Twenty-five pitfalls in the analysis of diffusion MRI data. NMR Biomed 2010;23(7):803-820.

[37] Xu J, Zhang L, Zhang D, Feng X. Multi-channel weighted nuclear norm minimization for real color image denoising. In: Proc IEEE Comput Soc Conf Comput Vis Pattern Recognit, 2017, p 1096-1104.

[38] Zhao Y, Liu Y, Mak HK, Wu EX. Simultaneous Denoising of Multi-contrast MR Images Using a Novel Weighted Nuclear Norm Minimization Approach. In: Proc of the 27th Annual Meeting of ISMRM, 2019, p 0669.

[39] Larsen T, Pryor G, Malcolm J. Jacket: GPU powered MATLAB acceleration. In: Hwu W-mW, editor. GPU Computing Gems. Jade ed: Elsevier; 2012. p 387-398.

Figure Captions

Figure 1. The proposed joint DWI dataset denoising consists of following steps: (1) for each 3D reference patch P_0 sliding across the 2D image region, searching similar patches (P_1, $P_{2, ...}$) through patch matching; stretching each reference patch together with its similar patches to vectors (y_0, y_1, $y_{2, ...}$) and concatenating them to form a patch matrix Y; (2) denoising the low-rank patch matrix via weighted nuclear norm minimization (WNNM), including singular value decomposition (SVD) to derive a diagonal matrix Σ, shrinking the singular values in Σ, and forming a denoised patch matrix X; (3) back-distributing each denoised patch matrix X into the 3D reference and similar patches ($P_0', P_1', P_2', ...$) in DWI space. Above three processes are repeated to all 3D reference patches. The final intensity of each DWI pixel is normalized by number of back-distributions to that specific pixel throughout the entire procedure.

Figure 2. Denoising results of the proposed method with simulated brain DWI/DTI dataset with 2% noise level. The dataset contained one b-value = 0 and 6 b-value = 1000 s/mm^2 images (for 6 directions). For simplicity, only one b-value = 1000 s/mm^2 image is shown. Denoising performance quantified in relative bias and NRMSE are shown in percentages. Noisy images were obtained by adding Rician noise to ground truth DWI images. The proposed method achieved more effective noise reduction than MPPCA method. The improved denoising results led to more accurate diffusion parametric maps.

Figure 3. Denoising results of our proposed method with simulated brain DWI dataset with 2% noise level. The dataset contained one b-value = 0 and 6 b-value = 2000 s/mm^2 images (for 6 directions). For simplicity, only one b-value = 2000 s/mm^2 image is shown. For these low SNR DWIs, the proposed method could achieve effective noise reduction while preserving structural details and produce more accurate diffusion parametric maps.

Figure 4. Denoising results with in vivo brain DWI dataset that consisted of one b-value = 0 and 6 b-value = 1000 s/mm^2 images in 6 directions. Only one DWI with b-value = 1000 s/mm^2 is shown. The dataset of NEX = 1 was used for denoising, while the dataset of NEX = 4 was used as a high SNR reference. The difference images were obtained by subtracting the denoised images from NEX = 4 reference images. The MD

and FA maps are displayed using the same scaling as in **Figure 2**. The proposed method achieved smaller NRMSEs in denoised DWIs as well as diffusion parametric maps (i.e., MD, FA and color-encoded FA).

Figure 5. Zoomed view of the denoising results in **Figure 4**. The proposed denoising results exhibited less residual noise than those using MPPCA. Note that apparent microstructural detail loss was observed in FA and color-encoded FA maps derived from the MPPCA denoised results as indicated by red and white arrows, respectively. In contrast, the proposed denoising led to more accurate FA and color-encoded FA maps, revealing more microstructural details that were comparable to those from NEX = 4 results.

Figure 6. Denoising results with in vivo brain DWI dataset that consisted of one b-value = 0 and 6 b-value = 2000 s/mm^2 images in 6 directions. Only one image with b-value = 2000 s/mm^2 is shown. The dataset of NEX = 1 was used for denoising, while the dataset of NEX = 10 was used as a high SNR reference. The difference images from NEX = 10 reference results are shown. The MD and FA maps are displayed using the same scaling as in **Figure 2**. At low SNR, the proposed method consistently outperformed MPPCA in terms of reducing noise while preserving structural details. It yielded diffusion parametric maps comparable to those from NEX = 4 results.

Figure 7. Zoomed view of the denoising results in **Figure 6**. Distinct noise was still present in MPPCA denoised DWI but largely absent in DWI denoised using the proposed method. The diffusion parametric maps derived from DWIs denoised using the proposed method again exhibited less noise and revealed more microstructural details (indicated by arrows).

Figure 8. Denoising results with in vivo brain multi-shell DWI dataset. The dataset consisted of one b-value = 0 image, and 6 diffusion directions with b-value = 1000/2000/3000 s/mm^2 (i.e., 19 images in total). Only one image per b-value is shown. The dataset of NEX = 1 was used for denoising, while the dataset of NEX = 4 was used as a high SNR reference. The difference images from NEX = 4 reference results are shown. The proposed method achieved more effective noise reduction in all DWIs (including the DWIs averaged from 6 diffusion directions per b-value), yielding approximately zero bias and 20% more NRMSE reduction compared to MPPCA.

Figure 9. Denoising results with reduced number of diffusion directions. Only one b-value = 0 and 3 b-value = 2000 s/mm^2 images (in 3 orthogonal diffusion directions) were extracted from the in vivo brain DWI dataset in **Figure 6**, and then denoised using ANLM and the proposed method. The ANLM results exhibited apparent blurring. In contrast, the proposed method achieved effective noise reduction while preserving structural details.

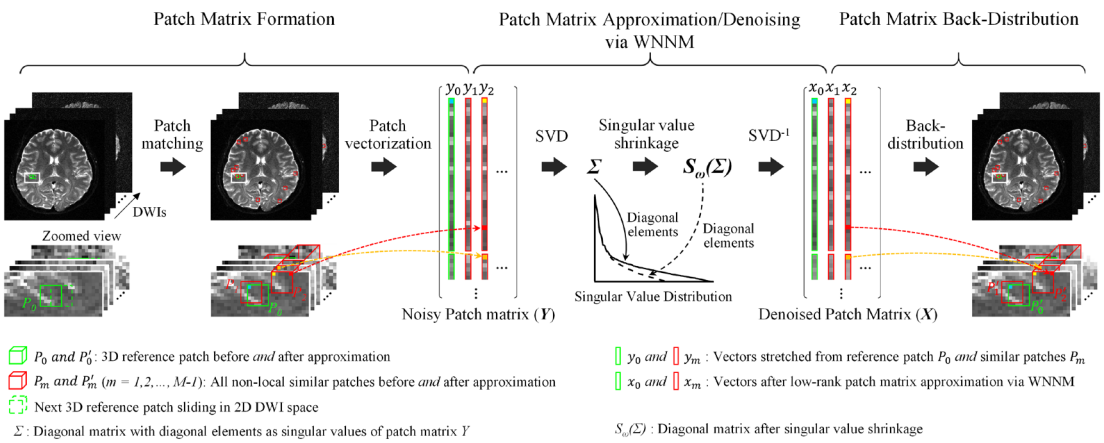

Figure 1

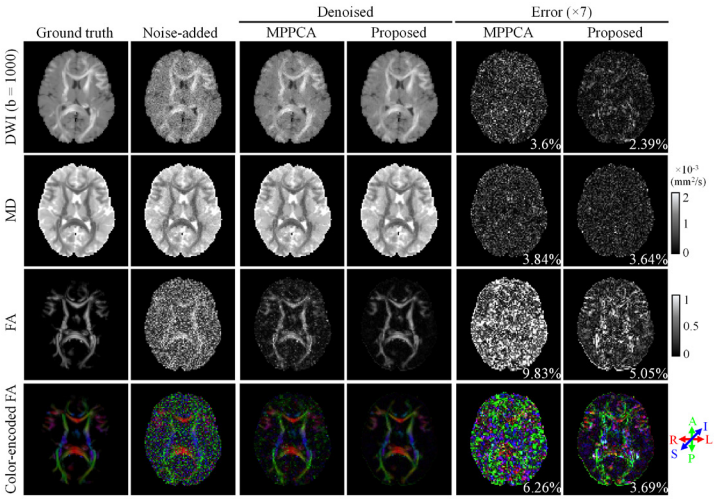

Figure 2

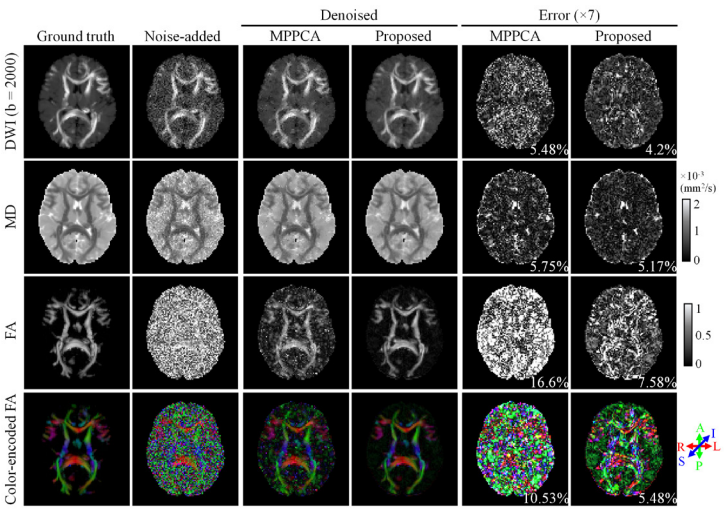

Figure 3

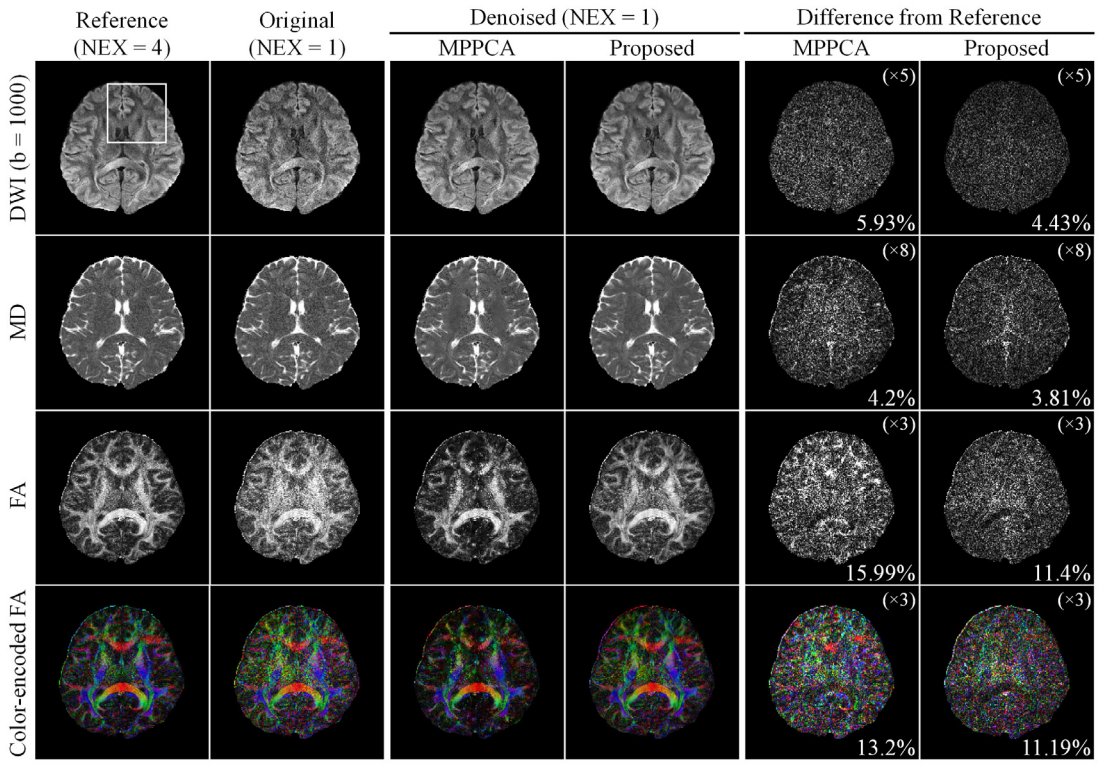

Figure 4

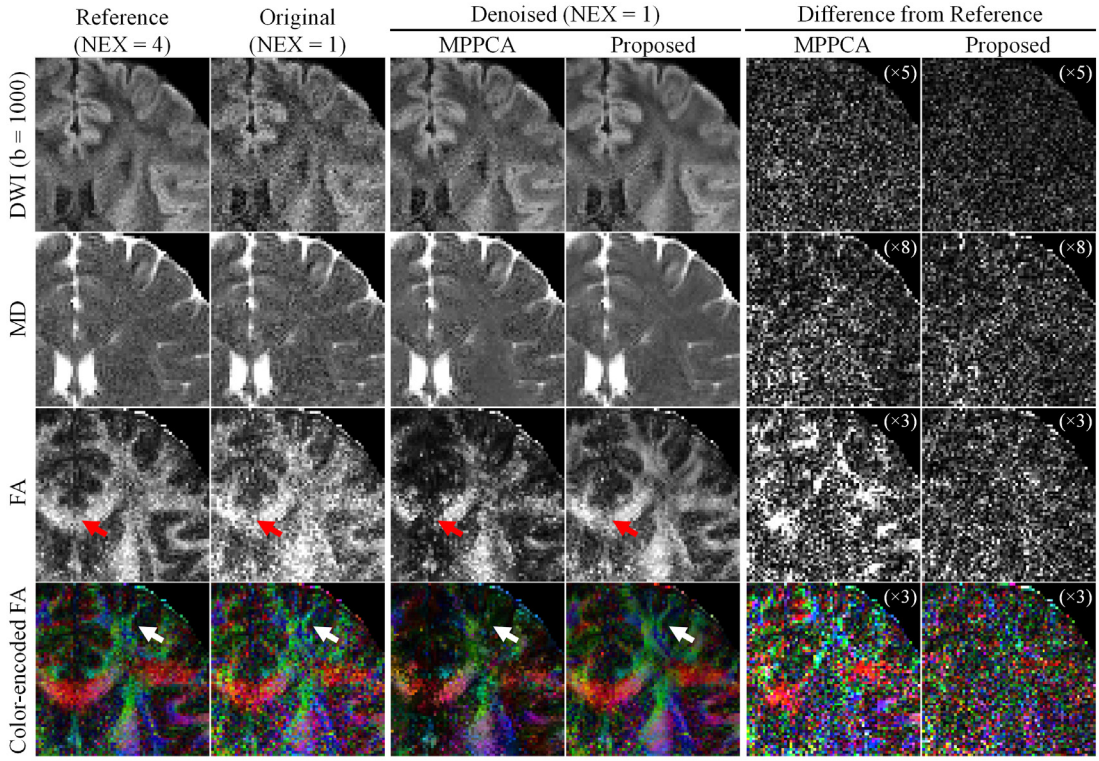

Figure 5

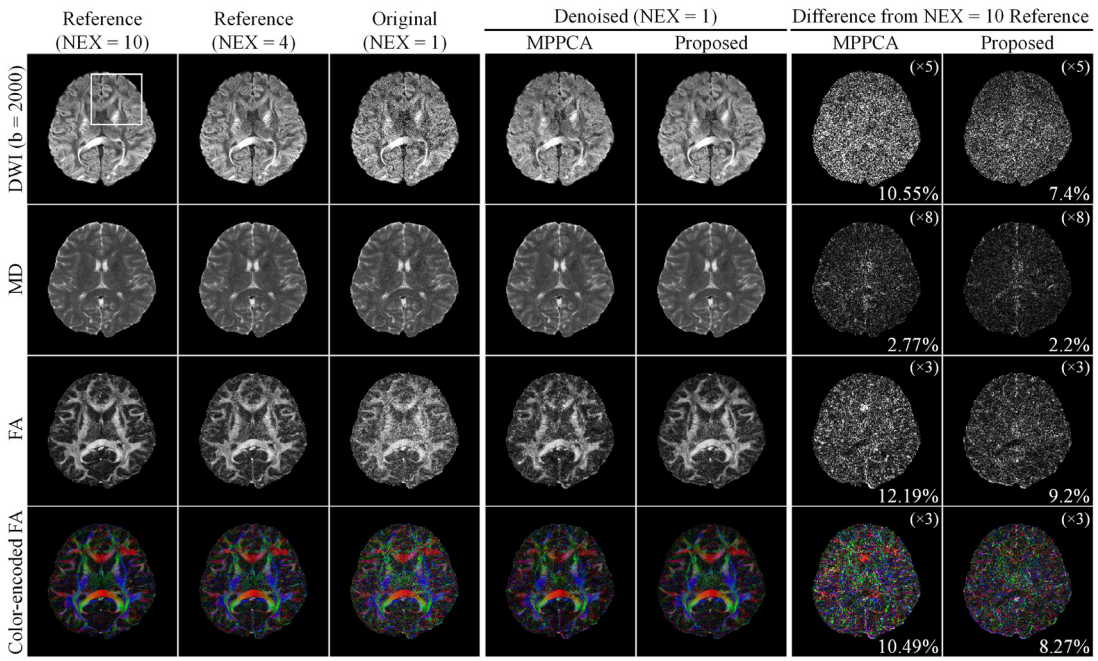

Figure 6

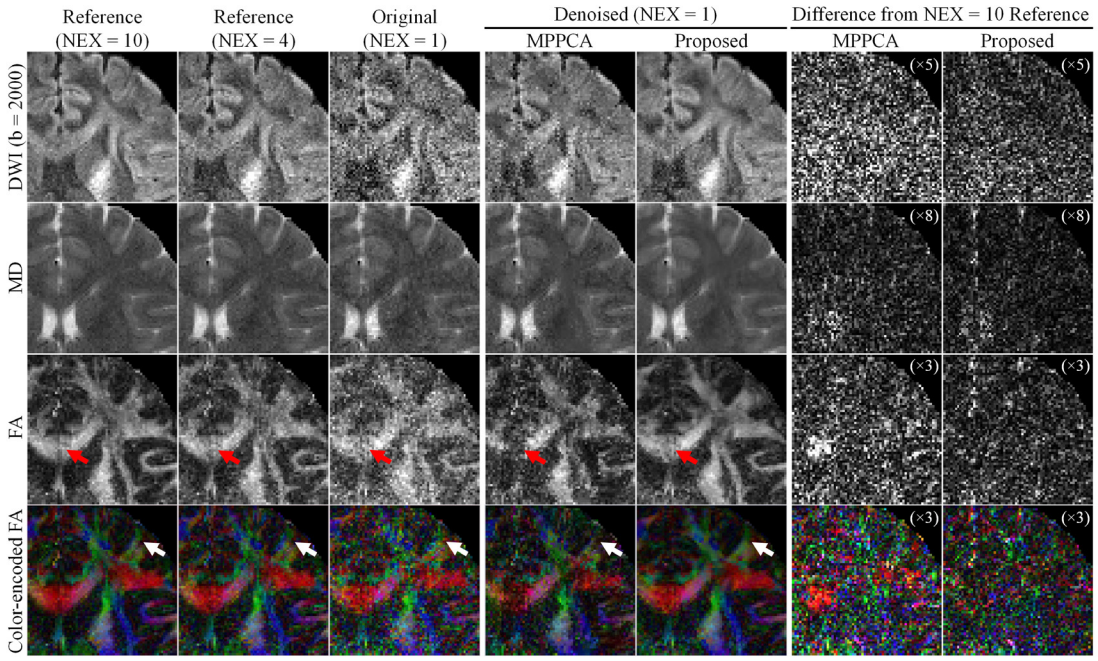

Figure 7

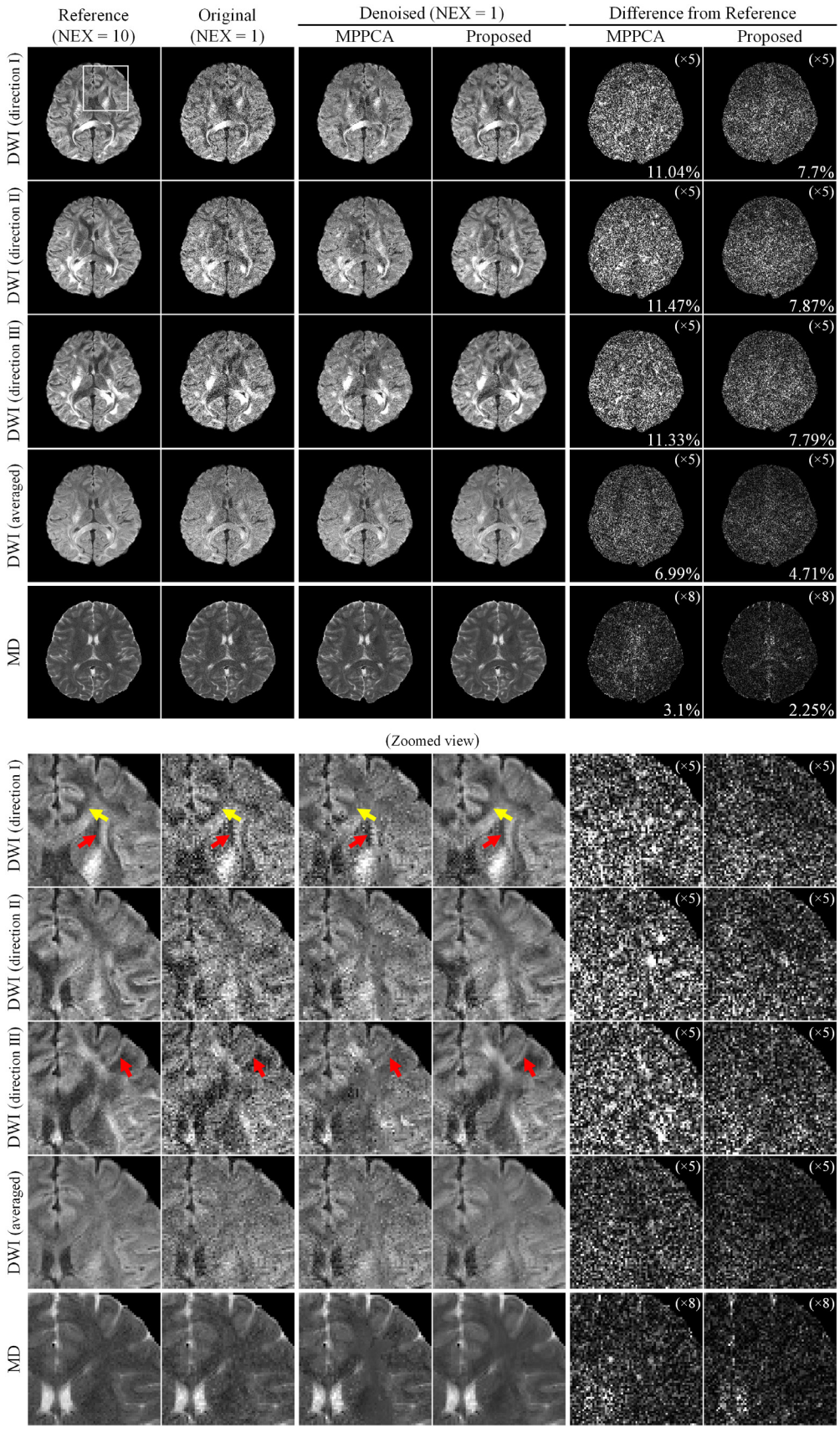
Reference (NEX = 10)
Original (NEX = 1)
Denoised (NEX = 1)
MPPCA
Proposed
Difference from Reference
MPPCA
Proposed
DWI (direction I)
DWI (direction II)
DWI (direction III)
DWI (averaged)
MD
(×5)
(×8)
11.04%
7.7%
11.47%
7.87%
11.33%
7.79%
6.99%
4.71%
3.1%
2.25%
(Zoomed view)

Figure 8